11th Canadian Masonry Symposium, Toronto, Ontario, May 31- June 3, 2009

ENERGY DISSIPATION CHARACTERISTICS OF INTERLOCKING GROUTED BRICK MASONRY

Maqsud E Nazar[1] and S.N. Sinha[2]
[1]Managing Director, NNC Consultant Pvt. Ltd., B-2, Jaswant Chambers, Okhla, Jamia Nagar, New Delhi-110025, India.
[2]Professor, Civil Engg. Department, Indian Institute of Technology, Delhi, New Delhi-110016, India.

ABSTRACT
A series of laboratory tests has been conducted to investigate the influence of bed joint orientation on interlocking grouted stabilised sand-flyash brick masonry under cyclic compressive loading. Five cases of loading at 0^0, 22.5^0, 45^0, 67.5^0 and 90^0 with the bed joints are considered. The brick units and masonry system developed by Prof. S.N. Sinha is used in present investigation. Eighteen specimens of size 500 mm x 100 mm x 700 mm (19.68 in. x 3.94 in. x 27.55 in.) and twenty seven specimens of size 500 mm x 100 mm x 500 mm (19.68 in. x 3.94 in. x 19.68 in.) are tested. The loops of stress-strain hysterisis obtained from cyclic loading tests have been used to determine the energy dissipation characteristics of interlocking grouted stabilised sand-flyash brick masonry. The variation of envelope strain, common point strain and stability point strain with plastic strain has been plotted. A polynomial formulation is proposed for the relations between energy dissipation ratio versus envelope strain and energy dissipation ratio versus residual strain. These relations indicates that the decay of masonry strength starts at about 0.42 to 0.75 times of peak stress depending upon the load case.

KEYWORDS: Interlocking brick, grout, uniaxial, cyclic loading, envelope curve, common point, stability point, stress-strain hysteresis.

INTRODUCTION
The behaviour of brick masonry under cyclic loading has been done in last couple of years by Naraine and Sinha [1], Choubey and Sinha [2], Milad and Sinha [3] and Senthivel and Sinha [4]. But, their findings were restricted to fired clay and sand plast bricks. Recently Singh and Sinha [5,6] investigated the cyclic behaviour of interlocking grouted stabilised mud brick / block masonry system developed by Prof. S.N. Sinha. Other researchers [7,8] also reported on the cyclic behaviour of brick masonry but in connection to seismic design of buildings with no particular emphasis into the cyclic deformation characteristics of masonry walls. Karsan and Jirsa [9] reported that plain concrete exhibits three fundamental stress-strain curves, when subjected to cyclic loading. It has similarly been found that brick masonry specimens also possess three similar stress-strain curves [1-6] under cyclic loading. The three stress-strain curves are termed as the envelope stress-strain curve, the common point stress-strain curve and

the stability point stress-strain curve.

Repeated loading-unloading cycles causes increase of residual strain that eventually produce failure. Abrams et al. [10] proposed that residual strains in the brick masonry assemblage can accumulate with application of load cycles that can lead to a splitting failure of a brick unit at a compressive stress less than the failure stress under monotonically increasing load. Test on brick masonry under cyclic loading gives useful information related to the material ductility, stiffness degradation, and energy dissipation characteristics.

The cumulative energy dissipation is often used as a measure of the structural seismic performance. The performance of reinforced concrete structure is widely measured by the concept of energy dissipation [11-13]. Low energy dissipation characterises the brittle behaviour of the structure while high energy dissipation indicates a ductile behaviour. Energy dissipation capacity has been used to assess the ability of a structural member to withstand cyclic loading in the inelastic range and serves as an indicator of the members capability to sustain damage without collapse [14-16].

Energy dissipation, usually expressed as a non-dimensional ratio [4,6,19,20] and defined as the energy dissipated per cycle to the total input energy. The test results indicate that the energy dissipation ratio, R_n increases linearly as a function of the imposed displacement at early loading stage. At the onset of cracks, the energy dissipation ratio shows a significant increase owing to the further increase in displacement. Senthivel and Sinha [4], Alshebani and Sinha [19] and Naraine and Sinha [20] have plotted the relation between energy dissipation ratio versus envelope strain and energy dissipation ratio versus plastic strain for conventional brick masonry. These curves are well comparable to each other but the plot between energy dissipation ratio versus envelope strain and energy dissipation ratio versus plastic strain obtained by Singh and Sinha [6] for interlocking grouted masonry is not comparable to similar curves drawn by Senthivel and Sinha [4], Alshebani and Sinha [19] and Naraine and Sinha [20]. Hence there is a need for more extensive study of energy dissipation characteristic of interlocking grouted brick masonry.

EXPERIMENTAL PROGRAM

TEST SPECIMEN

The test specimens of dimensions 500 mm x 100 mm x 700 mm (19.68 in. x 3.94 in. x 27.55 in.) and 500 mm x 100 mm x 500 mm (19.68 in. x 3.94 in. x 19.68 in) have been constructed from interlocking bricks of size 200 mm x 100 mm x 100 mm (7.87 in. x 3.94 in. x 3.94 in.) (Figure 1) developed by Prof. S.N. Sinha. The composition of brick units, grout and their compressive strength and standard deviation are given in Table 1, based on a test of 54 brick units and 48 mortar cubes.

Test specimens were made by the method developed by Prof. S.N. Sinha by interlocking bricks in stretcher bond. Layers of bricks were placed one after another without any mortar between them. It was self aligned due to interlocking of bricks. Then the cement grout was pump into the joints from the top, which spread all over and provided adequate bond. Three grout cubes of 70 mm (2.75 in.) size (control specimens) were also made for each specimen to determine the compressive strength of grout. The test specimens were built on 20 mm (0.79 in.) thick aluminium plates and cured under damp condition along with control specimens by covering with wet jute sacks for 28 days. All test specimens were leveled and capped with gypsum plaster before test.

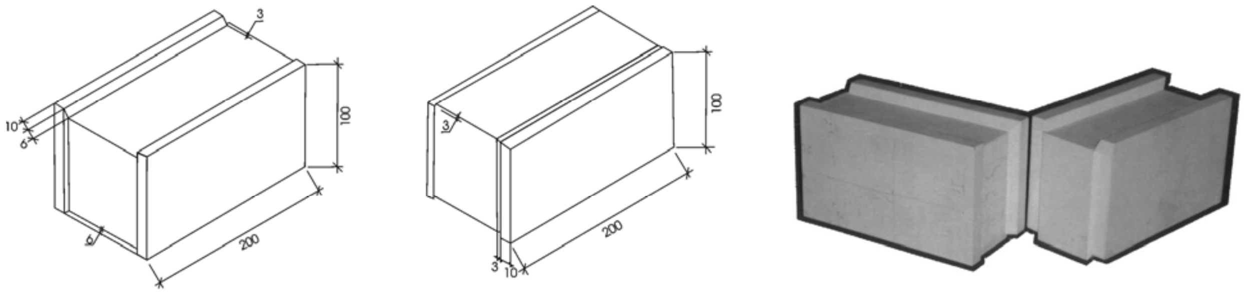

Figure 1: Interlocking

Table 1: Properties of Interlocking Bricks and Grout

Type of material	Mix proportion by weight	Water cement ratio	Mean compressive strength, MPa (psi)	Standard deviation, MPa (psi)
Interlocking stabilized sand-flyash brick	0.60 Coarse Sand : 0.25 Fly ash : 0.15 Cement	0.55	22.1 (3205.3)	1.53 (221.9)
Grout	Cement + Non- Shrink material @ 225 gm per 50 kg of cement (0.50 lb per 110 lb of cement)	0.4	38.3 (5554.9)	4.25 (616.4)

LOADING ARRANGEMENT

The interlocking brick masonry specimens were tested using a hydraulic servo controlled compression testing machine of 4000 KN (899 kips) capacity at a constant rate of displacement. To minimize the effect of platen restraint, Teflon sheets of 10 mm (0.40 in.) thickness were used on the two bearing surfaces of each specimen. The general loading arrangement and test set up are shown in Figure 2.

INSTRUMENTATION

The interlocking brick masonry specimens were instrumented for the measurement of axial and lateral displacements along fixed gauge lengths, using linear variable displacement transducers (LVDTs) on both sides of specimen. The gauge lengths for axial and lateral displacements were 350 mm (13.77 in.) and 250 mm (9.84 in.) respectively. Prior trials of different positions of LVDTs and gauge lengths arrangements indicate that the position of the LVDTs as shown in Figure 3 was the most appropriate. All LVDTs and load cell were connected to data acquisition system and a computer, where the displacement and load were recorded. The loading and unloading cycles were directly monitored from the on line display of load and displacement on monitor.

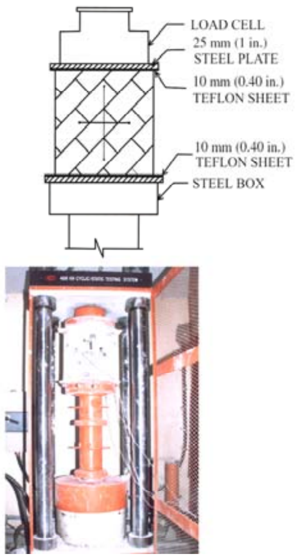

Figure 2: Loading Arrangement and Test Set up

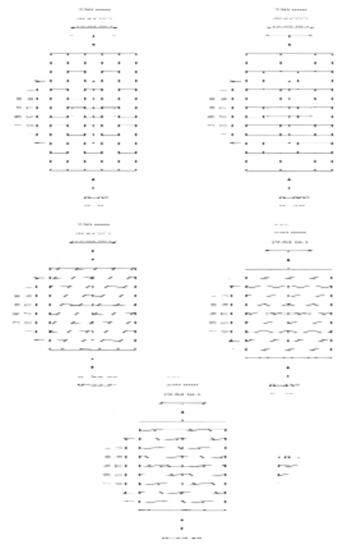

Figure 3: Arrangement of LVDTs and Loading Direction

TEST PROCEDURE

Test was conducted on 45 specimens under uniaxial cyclic compression. Five cases of loading at 0^0, 22.5^0, 45^0, 67.5^0 and 90^0 with the bed joints were considered. In each load case, three type of test were conducted. In first type of test, specimens were tested at a uniform rate of displacement to the failure of specimens. The rate of displacement was kept 0.01 mm ($4x10^{-3}$ in.) per second. In the second type of test, specimens were tested under cyclic loading in which loading and unloading were done several times, the peak stress-strain in each cycle of loading coincided approximately with monotonic envelope curve. The stress-strain curve so obtained possessed a locus of common points, where a common point is defined as the point at which the reloading curve of any cycle crosses the unloading curve of previous cycle (e.g. point A on Figure 4). In the third type of test, the cyclic load was applied as in the case of second type of test except that in each cycle, loading and unloading were repeated several times, each time unloading was done when the reloading curve intersected with the initial unloading curve, till the point of intersection gradually descended and stabilized, at lower bound (e.g. point B on Figure 5) and further cycling led to the formation of a closed hysteresis loop. Such lower bound points are termed as stability points.

The envelope stress-strain curves (Figure 6) were plotted for all five cases of loading and obtained by super imposing the data from first type of test and peaks of stress-strain curves from second and third type of tests. The stability point curves (Figure 22) were also plotted for all five cases of loading obtained from third type of test.

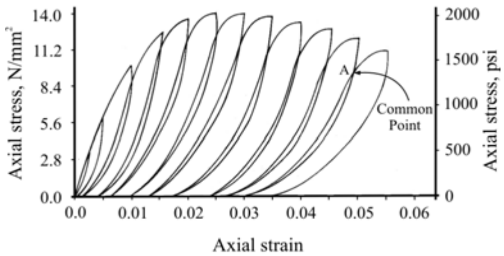

Figure 4: Typical Test under Cyclic Loading for Common Points

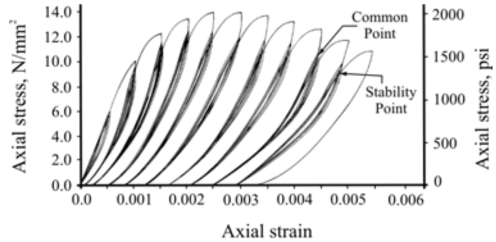

Figure 5: Typical Test under Cyclic Loading for Stability Points

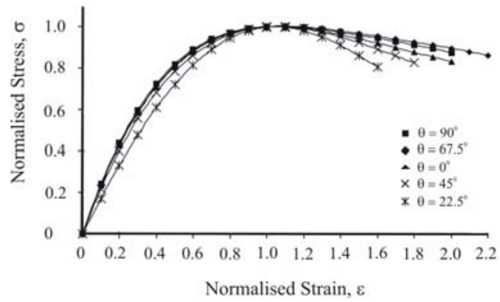

Figure 6: Analytical Envelope Curves

TEST RESULTS AND EVALUATION

FAILURE MODES

Crack initiations of the interlocking grouted stabilized sand-flyash brick masonry specimens varied according to the load cases. For specimens, loaded parallel to bed joint (i.e. specimens loaded at 0^0 to the bed joints), cracks initiated at bed joints. The splitting initiates at free edges and gradually propagates towards the centre of panel. Thereafter, the separated fragments of the panel behave like individual compression members. For specimens loaded normal to bed joints (i.e. specimens loaded at 90^0 to the bed joints), cracks initiated at the head joints and bed joints followed by cracks in the bricks. Failure in this case occurred by a mechanism that usually involved a combination of brick failure and joint failure. Failure also occurred perpendicular to plane of the specimen characterised by formation of the tensile cracks parallel to axis of loading.

The test specimens loaded at 22.5^0 to the bed joints displayed a failure pattern that was confined to joints, whereas the specimens loaded at 45^0 to the bed joints exhibited partial bond failures in joints accompanied by splitting of bricks. In case of specimens loaded at 67.5^0 to the bed joints, failure modes were similar to that observed in specimens loaded normal to bed joints. Typical failure pattern of specimens observed during experimental investigation are shown in Figure 7.

ENERGY DISSIPATION CHARACTERISTICS

The most important aspect of structural performance under cyclic loading is the ability of the structure to adequately dissipate energy. Energy dissipated per cycle of loading has been expressed as a dimension less ratio, R_n. The energy dissipation ratio, R_n is defined as the ratio of the energy dissipated per cycle to the total energy as diagrammatically shown in Figure 8 for typical reloading-unloading cyclic curve. The energy dissipated per cycle represents the area enclosed by the reloading-unloading loop of that cycle. The total input energy per cycle is the total stored strain energy per cycle of reloading-unloading curve. The area under the curves is calculated by averaging the readings of a digital planimeter.

The plastic (residual) strain in the brick masonry is useful parameter for determining the permissible stress level. Hence the variation of plastic strain with envelope strain, common point strain and stability point strain also discussed along with energy dissipation ratio versus envelope strain and energy dissipation ratio versus plastic strain.

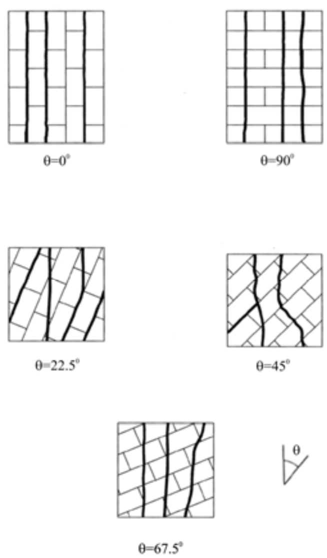

Figure 7: Modes of Failure

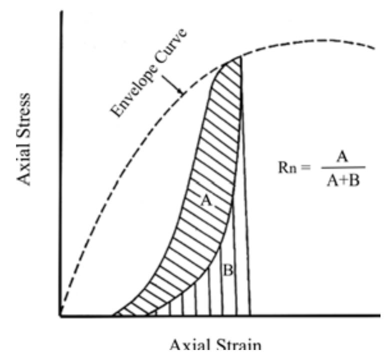

Figure 8: Determination of Rn

VARIATION OF PLASTIC STRAINS

Plastic (residual) strains accumulate as the number and intensity of load cycles increase. The plastic strain ε_r at the end of unloading, are plotted against the envelope strain at the beginning of unloading ε_E in Figure 9 for all five cases of loading. The variation of ε_r versus ε_E is presented in non-dimensioned co-ordinate system. The plastic strain and envelope strain are each normalised with respect to ε_m, the strain corresponding to peak stress. The variation of non-dimensional plastic-strain at the end of unloading against the non-dimensional strain at the common point ε_c and against the non-dimensional strain at stability point ε_s are plotted in Figure 10 and Figure 11 respectively.

Based upon the experimental data, the variations of ε_r versus ε_E, ε_c and ε_s can be predicted by a general polynomial equation as,

$$\varepsilon_r = \alpha\varepsilon^2 + \beta\varepsilon \qquad (1)$$

where,

ε_r = normalised residual (plastic) strain

ε = normalised strain at envelope, ε_E, at common point ε_c and stability point ε_s

α and β = equation's constants.

The values of α, β and correlation index i_c are given in Table 2. The correlation index i_c for equation (1) ranges from 0.9512 to 0.9830, an indicative of good agreement between test data and the analytical curves.

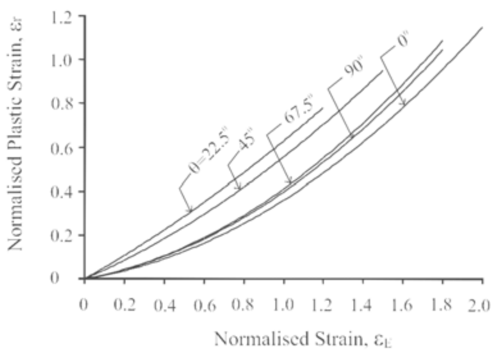

Figure 9: Variation of Envelope Strain with Plastic Strain

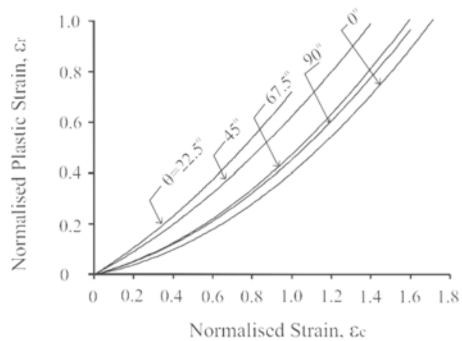

Figure 10: Variation of Common Point Strain with Plastic Strain

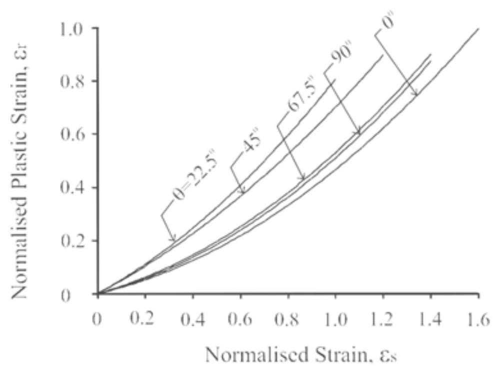

Figure 11: Variation of Stability Point Strain with Plastic Strain

R_n VERSUS ENVELOPE STRAIN

The energy dissipation ratio (R_n) determined for each cycle of loading-unloading are plotted against the normalised strain at the peak of each cycle and shown in Figs. 12 to 16 for specimens loaded at 0^0, 22.5^0, 45^0, 67.5^0 and 90^0 to the bed joints respectively.

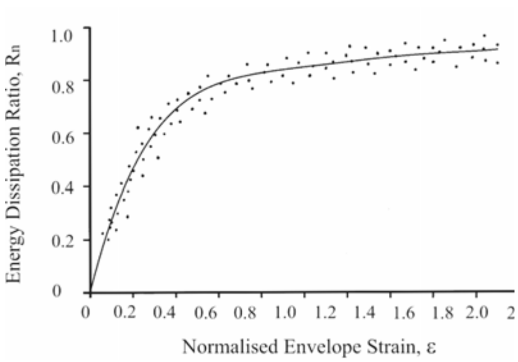

Figure 12: Rn versus Envelope Strain ($\theta=0^0$)

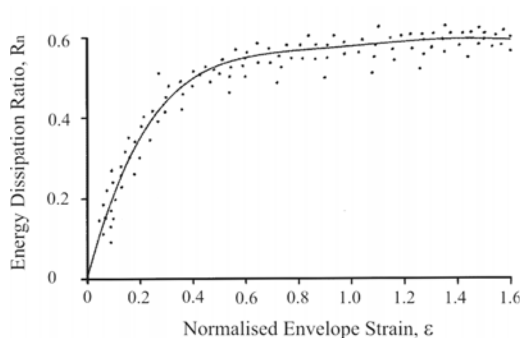

Figure 13: Rn versus Envelope Strain ($\theta=22.5^0$)

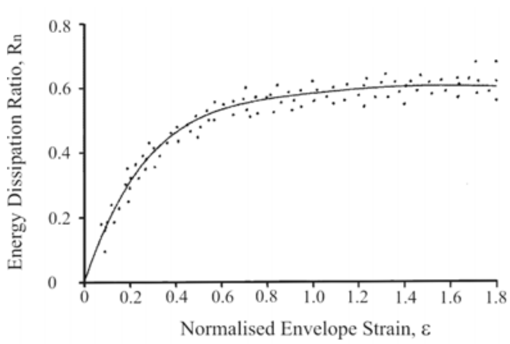

Figure 14: Rn versus Envelope Strain ($\theta=0^0$)

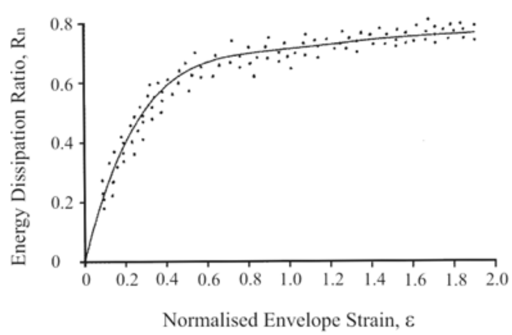

Figure 15: Rn versus Envelope Strain ($\theta=0^0$)

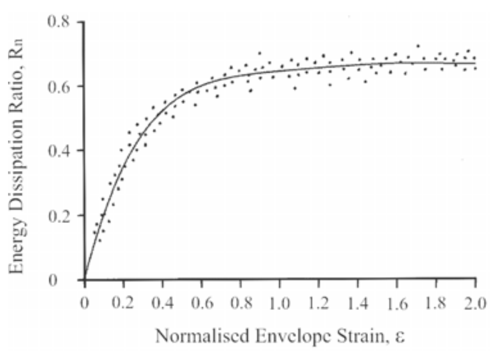

Figure 16: Rn versus Envelope Strain ($\theta=90^0$)

Table 2: Values of α, β and i_c for Plastic Strain vs Envelope, Common Point and Stability Point Strain

Plastic strain variation curves	Load case with respect to bed joint orientation, θ	Equation Parameters		Correlation index, i_c
		α	β	
εr versus ε_E	0^0	0.2153	0.1435	0.9710
	22.5^0	0.1148	0.5127	0.9670
	45^0	0.1585	0.3961	0.9634
	67.5^0	0.2422	0.1676	0.9685
	90^0	0.2304	0.1660	0.9812
εr versus εc	0^0	0.2586	0.1433	0.9712
	22.5^0	0.2377	0.4834	0.9513
	45^0	0.2111	0.4128	0.9765
	67.5^0	0.2642	0.2099	0.9532
	90^0	0.2517	0.2023	0.9512
εr versus εs	0^0	0.2610	0.2071	0.9632
	22.5^0	0.3222	0.4881	0.9683
	45^0	0.2305	0.4733	0.9830
	67.5^0	0.2812	0.2512	0.9683
	90^0	0.2854	0.2268	0.9732

Based upon the experimental data following mathematical expression is proposed.

$$R_n = a\varepsilon_E^5 + b\varepsilon_E^4 + c\varepsilon_E^3 + d\varepsilon_E^2 + e\varepsilon_E \tag{2}$$

where,
R_n = energy dissipation ratio; ε_E = normalised envelope strain, $\varepsilon_a / \varepsilon_m$; a,b,c,d and e = equation's constant

By assigning suitable values of a, b, c, d and e the equation is used to obtain the energy dissipation ratio, R_n for interlocking grouted stabilised sand-flyash brick masonry. Table 3 gives the values of a, b, c, d , e and correlation index, i_c for different load cases. The correlation index, i_c is in the range of 0.912 to 0.971 for all five cases of loading indicate good corelation.

In, general, the variation of energy dissipation ratio, R_n with envelope strain exhibits three zones. An initial linear portion with high rate of increase of R_n and low rate of increase in strain followed by a transit non-linear portion and then followed by a relatively approximate linear portion with slower rate of increase in R_n and faster rate of increase in strain ratio. The relatively high rate of increase of energy dissipation ratio, R_n at the initial stages of cyclic loading can be associated with the formation of micro-cracks in the brick masonry specimens. Subsequently, the rate of increase of R_n decreases which may be associated with the widening of the micro-cracks. The initial linear portion of R_n versus ε_E curves can be associated with the elastic response of the material, since the formation of micro-cracks does not result in much accumulation of plastic (residual) strain.

The energy dissipation ratio, R_n increases approximately linearly up to 0.44, 0.37, 0.36, 0.42 and 0.38 for specimens loaded at 0^0, 22.5^0, 45^0, 67.5^0 and 90^0 to bed joints respectively. The corresponding strain ratios were 0.20, 0.25, 0.22, 0.20 and 0.20 respectively.

From the envelope stress-strain relations presented in Figure 6, for envelope strain ratio of 0.20, 0.25, 0.22, 0.2 and 0.2 for specimen loaded 0^0, 22.5^0, 45^0, 67.5^0 and 90^0 respectively, the corresponding stress ratios are 0.44, 0.42, 0.44, 0.44 and 0.44 respectively. The envelope stress-strain curve (Figure 6) is also observed to be approximately linear up to stress ratio of 0.44, 0.42, 0.44, 0.44 and 0.44 for specimens loaded at 0^0, 22.5^0, 45^0, 67.5^0 and 90^0 to bed joints. Hence from the energy dissipation characteristics, it can be hypothesized that a stress ratio of 0.44, 0.42, 0.44, 0.44 and 0.44 for specimens loaded at 0^0, 22.5^0, 45^0, 67.5^0 and 90^0 can be used as elastic limit for interlocking grouted stabilised sand-flyash brick masonry.

From the plastic strain curves ε_r versus ε_E (Figure 9) unloading from an envelope strain ratio of 0.20 for specimens loaded at 0^0, 67.5^0 and 90^0 to bed joints, results in a plastic (residual) strain ratio in the range of 0.03 to 0.04. For the envelope strain ratio of 0.22 for specimen loaded at 45^0 to bed joints correspond to plastic strain ratio is 0.09. These extremely low levels of plastic strain also confirms an elastic response of material. From Figure 9, unloading from an envelope strain ratio of 0.25, results in a plastic strain ratio is 0.13 for specimen loaded at 22.5^0 to the bed joints. This is high plastic strain ratio as compared to plastic strain ratios obtained for other load cases. This could be due to slipping of joints at early stage of loading.

R_n VERSUS RESIDUAL STRAIN

The energy dissipation ratio, R_n versus the plastic strain ratio, ε_r are plotted in Figs. 17 to21 for all five cases of loading. Based upon the experimental data. Following polynomial formulation is proposed,

$$R_n = a\varepsilon_r^5 + b\varepsilon_r^4 + c\varepsilon_r^3 + d\varepsilon_r^2 + e\varepsilon_r \qquad (3)$$

where,
R_n = energy dissipation ratio; ε_r = plastic (residual) strain ratio; a,b,c,d,e = equation's constants

The values of a, b, c, d, e and correlation index, i_c are given in Table 3.

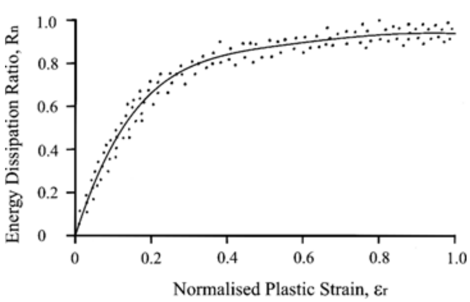

Strain ($\theta=0^0$)

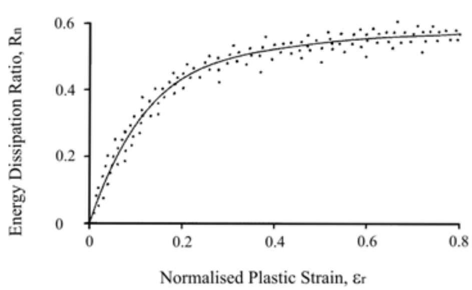

Strain ($\theta=22.5^0$)

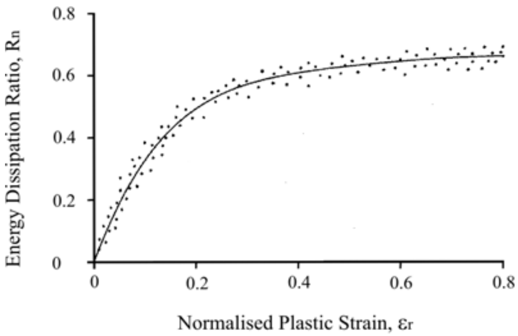

Figure 19: Rn versus Plastic Strain (θ=22.5^0)

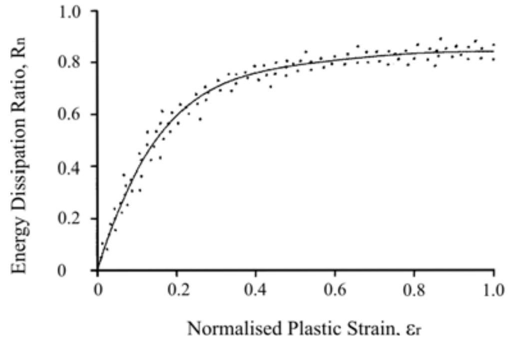

Figure 20: Rn versus Plastic Strain (θ=45^0)

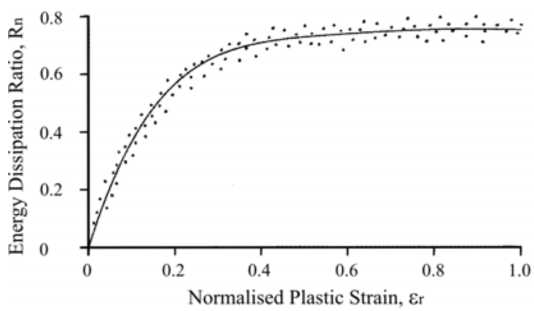

Figure 21: Rn versus Plastic Strain (θ=90^0)

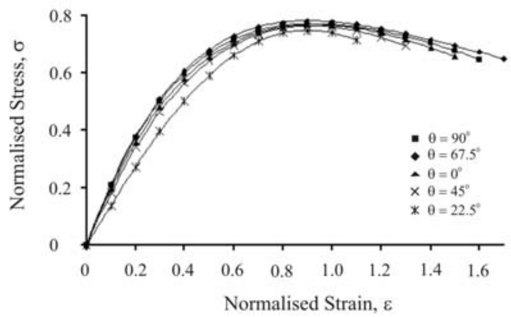

Figure 22: Analytical Stability Point Stress-Strain Curves

It may be observed that the relationship between R_n and ε_r is bilinear and similar to that between R_n and ε_E. A higher rate of increase in R_n is observed at early stages of loading when only micro-cracks form, with insignificant accumulation of plastic strain. A slower increase in R_n with faster increase in ε_r at later stages of loading reflects the growing and widening of cracks and thus faster accumulation of plastic strain.

An approximately linear relationship exist between R_n and ε_r upto a plastic strain ratio (ε_r) of approximately 0.08, 0.13, 0.12, 0.08 and 0.08 for specimens loaded at 0^0, 22.5^0, 45^0, 67.5^0 and 90^0 to bed joints respectively. From plastic strain versus envelope strain curves (Figure 9) for specimens loaded at 0^0, 22.5^0, 45^0, 67.5^0 and 90^0 to the bed joints, the values of ε_r of 0.08, 0.13, 0.12, 0.08 and 0.08 corresponds to a value of ε_E of 0.42, 0.25, 0.30, 0.40 and 0.40 respectively. The later may corresponds to an envelope stress ratio of 0.73, 0.42, 0.55, 0.74 and 0.75 for specimen loaded at 0^0, 22.5^0, 45^0, 67.5^0 and 90^0 to the bed joints respectively. These stress ratios are also in close proximity with the peak stress ratios predicted by the stability point curves (Figure 22) for specimen loaded at 0^0, 67.5^0 and 90^0 to the bed joints. But for the specimen loaded at 22.5^0 and 45^0 to the bed joints envelope stress ratios of 0.42 and 0.55 respectively are obtained against the stability point peak stress ratios of 0.745 and 0.76 respectively. This lower value of stress ratio could be due to the slipping of joints at early stage of loading for these two load cases. The point where non-linearly in plastic strain begins to occur may be interpreted as the point in the loading history denoting the beginning of the process of deterioration of the micro-cracks in the material. Hence from the energy dissipation characteristics, it can be hypothesized that the peak of stability point stress can be used as damage indicator of the material.

Table 3: Values of a, b, c, d, e and i_c for R_n vs ε_E and R_n vs ε_r curves

Energy Dissipation Curve	Load Case with respect to bed joint orientation, θ	Equation Parameters					Correlation index, i_c
		a	b	c	d	e	
R_n versus ε_E	0^0	0.2360	-1.5448	3.9489	-4.9586	3.1654	0.930
	22.5^0	-0.2657	-1.6259	-3.8209	-4.3497	-4.3497	0.921
	45^0	0.1566	-1.0074	2.5365	-3.1867	2.0834	0.935
	67.5^0	0.2074	-1.3674	3.5066	-4.3841	2.7503	0.965
	90^0	0.1401	-0.9718	2.6258	-3.4868	2.3368	0.945
R_n versus ε_r	0^0	3.8991	-14.528	21.047	-15.072	5.5931	0.933
	22.5^0	8.6697	-23.766	25.815	-14.167	4.143	0.951
	45^0	5.2137	-16.703	21.066	-13.309	4.4079	0.937
	67.5^0	3.3700	-12.453	18.095	-13.138	4.9645	0.926
	90^0	3.1479	-11.921	17.651	-12.925	4.7985	0.956

The energy dissipation ratio versus envelope strain and energy dissipation ratio versus plastic strain curves and inferences drawn in this study is similar to those obtained by Senthivel and Sinha [4], Alshebani and Sinha [19] and Naraine and Sinha [20]. The energy dissipation ratio versus envelope strain and energy dissipation ratio versus plastic strain curves obtained by Singh and Sinha [6] for interlocking grouted stabilised mud blocks under cyclic loading with specimens loaded at 0^0 and 90^0 to bed joints are not comparable to this study.

CONCLUSION

Following conclusions are made from the results obtained from the investigation on the behaviour of interlocking grouted stablised sand-flyash brick masonry under uniaxial cyclic compressive loading.

1. The stress-strain hysterisis of the cyclic loading can be used to study the energy dissipation capacity of interlocking grouted stabilised sand-flyash brick masonry.

2. The energy dissipation ratio, R_n is plotted with respect to normalised envelope strain and normalised plastic strain for all five cases of loading. These plots exhibited bilinear behaviour with initial linear high rate of increase in R_n followed by short non-linear transit portion and then a relatively approximate linear slower rate of increase in R_n and a higher increase in strain.

3. The initial linear portion of R_n versus ε_E can be associated with the elastic response of material since the formation of micro-cracks does not result in much accumulation of plastic strain. Subsequently, the rate of increase in R_n decreases which may be associated with the widening of the micro-cracks.

4. The relation between R_n and ε_r can be used to identify the point of load history at which the process of strength deterioration begins. The stress at this point is in close approximity to the peak stress of the stability point curve. It is about 0.73 to 0.75 times the failure (peak) stress for specimens loaded at 0^0, 67.5^0 and 90^0 to bed joints. But it is 0.42 and 0.55 times the failure (peak) stress for specimens loaded at 22.5^0 and 45^0 to bed joints respectively. Hence, from the energy dissipation characteristics of interlocking grouted stabilised sand-flyash brick masonry, it can be hypothesized that the peak of the stability stress can be used as damage indicator of the material.

REFERENCES

1. Naraine, K. and Sinha, S.N. (1989), "Behaviour of brick masonry under cyclic compressive loading", Journal of Structural Engineering, ASCE.

2. Choubey, U.B. and Sinha, S.N. (1991), "Cyclic Compressive loading response of brick masonry". Journal of Masonry International.

3. Milad, M.A. and Sinha S.N. (1999), "Stress-Strain Characteristics of brick masonry under uniaxial loading", Journal of structural Engineering, ASCE.

4. Senthivel, R. and Sinha S.N. (2003), "Energy dissipation response of brick masonry under cyclic compressive loading", Structural Engineering and Mechanics.

5. Singh, B.K. and Sinha S.N. (2004), "Stress-Strain Curves for Interlocking Grouted Stablised Mud Brick Masonry in Cyclic Uniaxial Compressive Loading", The Third International Conference on Advances in Structural Engineering and Mechanics, Seoul, Korea.

6. Singh, B.K. and Sinha S.N. (2004), "Energy dissipation in interlocking grouted stabilized mud block masonry under cyclic uniaxial compressive loading", 13th International Brick and Block Masonry Conference, Amsterdam.

7. Chen, S.W.J., Hidalgo, P.A., Mayes, R.L., Clough, R.W. and McNiven, H.D. (1978), "Cyclic loading test of masonry single piers, volume 2 - Height to width ratio 1". EERC Rep. No. 78/28, Envir. Engrs. Res. Council, University of California, Berkley, California.

8. Macchi, G. (1985), "Behaviour of masonry under cyclic actions and seismic design". Proc. International Brick Masonry Conference.

9. Karsan, J.K. and Jirsa, J.O. (1969), "Behaviour of Concrete under compressive loading". J. Street Div., ASCE.

10. Abrams, D. Noland, J. and Atkinson, R. (1985), "Response of clay unit masonry to repeated compressive forces". Proc. 7th Int. Brick. Masonry Conference, Melbourne.

11. Hwang, T.H. and Scribner, C.F. (1984), “R/C member cyclic response during various loadings”, J. Struct. Div., ASCE.

12. Darwin, D. and Nmai, C.K. (1986), “Energy dissipation in RC beams under cyclic loads”, J. Struct. Div., ASCE.

13. Bertero, V.V. and Popov, E.P. (1977), “Seismic behaviour of ductile moment resisting reinforced concrete frames”, Reinforced Concrete Structures in Seismic Zones, SP-53, American Concrete Institute, Detroit.

14. Banon, H., Biggs, J.M. and Irvine, H.M. (1981), “Seismic behaviour of ductile moment resisting reinforced concrete frames”, J. Struct. Div., ASCE.

15. Brown, R.H. and Jirsa, J.O., Reinforced Concrete Beams under Load Reversals, “J. of American Conc. Inst.

16. Gosain, N.K., Brown, R.H. and Jirsa, J.O. (1977), “Shear requirements for Load Reversals on RC Members”, Journal of Structural Engineering Division, ASCE.

17. Hidalgo, P.A., Mayes, R.L., McNiven, H.D. and Clough, R.W. (1978), Cyclic Loading Tests of Masonry single piers, Vol-I-Height to width ratio of 2” EERC Report No. 78/28, University of California, Berkeley.

18. Byong, Y.B. and Cheng-Tzu. (1998), “Stress-Strain behaviour of concrete under cyclic loading”. ACI Materials Journal.

19. Alshebani, M.M., and Sinha, S.N. (2000), “Energy dissipation of masonry under cyclic biaxial compression”, Int. Conference on Structures under Shock and Impact-IV, Wessex Institute of Technology, London.

20. Naraine, K., and Sinha, S.N. (1989), “Energy Dissipation in Brick Masonry under Cyclic Compressive Loading”, Second International Masonry Conference, London.